An integrated biological analysis and flow rate sensing for the real-time detection of carcinogen in water based on Co^{2+}-doped optical fibers

Ran Gao, Jiansen Ye, and Xiangjun Xin

***Abstract*—The multi-parameter measurement has significant meaning for biosensor to enhance their practical sensing performance. For the biological detection, simultaneous measurement of biological molecule and flow rate could improve the accuracy and sensitivity of sensors significantly. In this paper, an integrated biological analysis and flow rate sensing based on Co^{2+} doped tilted fiber Bragg gratings has been proposed and experimentally demonstrated for real-time the detection of the Benzo[a]pyrene molecules. A tilted fiber Bragg grating with a tilted angle of 8º was inscribed into a Co^{2+} doped fiber. The flow rate and Benzo[a]pyrene molecules can be measured simultaneously by interrogating the resonance wavelength of core mode and wavelength interval between the core mode and cladding mode according to the heat exchange and evanescent field of the cladding mode, respectively. Experimental results show that the real-time measurement sensitivities of 12 pm/pM and -0.13 nm/(μL/s) for the Benzo[a]pyrene detection and flow rate were achieved, respectively. Thus the technique appears to have potential applications in chemistry, medicine, and biology.**

***Index Terms*—Benzo[a]pyrene detection, Co^{2+} doped tilted fiber Bragg gratings, Flow rate measurement, Thermal effects.**

I. Introduction

BENZO[A]PYRENES (B[a]P) are formed during the incomplete burning of coal, oil, gas, wood, garbage, or other organic substances [1]. B[a]P is one kinds of carcinogens, acting as endocrine-disrupting compounds [2]. The maximum allowed limits of B[a]P in drinking water have been rigid ruled less than 10 ng/L in many countries and regions [3-5]. Hence, the detection of B[a]P is widely used in various applications, such as environment protection, medicine, and bioengineering, etc.

Optical biosensors have received considerable attention due to their advantages of high sensitivity and low cost. Therefore, various sensing methods have been developed for sensitive B[a]P determination in the past, such as surface enhanced Raman spectroscopy (SERS) [6, 7], surface-plasmon resonance (SPR) [8, 9], and fluorescence spectroscopy [10]. Especially, the dense gold film was replaced by a nanoporous gold film in the nanoporous gold film based SPR. The nanoporous gold film not only improves the adsorption of the B[a]P molecules, but also enhances the interaction between the B[a]P molecules and the optical field, which improves the sensitivity of the B[a]P detection effectively [11]. Compared with conventional optical sensors, the label-free fiber optic immunoreactions biosensors could also study the kinetics of biomolecular interactions with low cost and real time, including DNA, molecule, and proteins, etc. [12]. Many miniaturized fiber biosensor have been researched, such as various lab-on-fiber technology [13], including lab-on-tip (plasmonic optical fiber probes or SERS-based probes) [14], lab-around-fiber (tapered fiber and fiber grating) [14], and lab-in-fiber (photonic crystal fiber) [14]. Another promising fiber biosensor is based on micro-cantilever [15]. Biomolecular interactions on one side of a cantilever surface can be transferred to mechanical bending due to differential surface stress change or resonant frequency shift of the cantilever. The fiber micro-cantilever biosensor can provide rapid, reliable sensing platform, which can potentially not only be portable but also using minimal quantities of biological sample volumes. Tilted fiber Bragg gratings (TFBGs), in which the refractive index (RI) modulation is slightly angled with respect to the optical fiber propagation axis, generate the self-backward coupling of the core mode and numerous backward couplings between the core mode and different cladding modes [16]. The evanescent field of the cladding mode presents its own sensitivity to the surrounding RI. Due to its limited penetration depth, an evanescent field can interact selectively with the molecules at the interface without interference from the free molecules in solution. Hence many TFBGs based biochemical sensors have been developed. B. B. Luo presented a human heart failure biomarker immunosensor based on excessively tilted fiber gratings [17]. C. Ribaut developed a cytokeratin 7 of lung cancer biomarkers by using SPR-TFBG [18]. A. L. Aldaba reported an optical fiber pH sensor based on a polyaniline coated TFBG [19].

The measurement of flow rate also plays a very important

The paper was submitted for review on July 12, 2019. This work was supported by the National Natural Science Foundation of China (NSFC) (61601436) and Cultivating funding of Zhengzhou Institute of Technology (No. GJJKTPY2018K3).

Ran Gao and Xiangjun Xin was with Advanced Research Institute of Multidisciplinary Science, Beijing Institute of Technology, Beijing 100081, China. (e-mail: gaoran198412@163.com, xjxin@bupt.edu.cn). Jiansen Ye was with School of Information Engineering, Zhengzhou Institute of Technology, No.18 yingcai street, huiji district, Zhengzhou, 450044. (e-mail: forest929@163.com).

This article has been accepted for publication in a future issue of this journal, but has not been fully edited. Content may change prior to final publication. Citation information: DOI 10.1109/JSEN.2019.2948964, IEEE Sensors Journal

role in label-free immunoreactions biosensors. In general, the immunoreactions between the antibody and B[a]P molecule can be described as two steps according to the intrinsic adsorption kinetics [20]: the transmission process of the B[a]P molecule from the bulk solution to the surface of the fiber, and the absorption process between the antibody and the B[a]P molecule. Therefore, most of immunosensors always stand the bio-sample for tens of minutes in order to wait for the complete immobilization on the surface of the sensor [17-19]. However, real-time optical biosensors need the rapid detection of different bio-samples *in suit* with tens of seconds. Hence the simultaneous measurement of the bio-sample and flow rate is very important for the real-time integrated biosensor to balance the immunoreaction and the flow rate [21]. Besides, many microfluidic devices need the precise and accurate control of flow rate in order to increase the interaction between bio-sample and antibody or enhance the isolation/ separation. For example, in the herringbone microfluidic chip, the herringbone-induced microvortices disrupt the laminar flow streamlines that cells travel, causing the circulating tumor cells to "shift", increasing the number of cell-surface interactions in the antibody-coated device [22]. The experimental results show that the capture efficiency of the herringbone microfluidic chip is highly dependence of the flow rate. Therefore, the measurement of flow rate is critical in the optical biosensors, which could improve the efficiency and accuracy of biosensors significantly.

The most well-known fiber flowmeter is the "hot-wire", which is based on the heat exchange between the heated source and flowing liquid. However, most of fiber flowmeters could only detect the liquid flow rate, such as the self-heated Co^{2+}-doped fiber Bragg fiber (FBG) [23, 24], silver coated FBG assisted by a no-core fiber [25], and Fabry-Pérot silicon interferometer heated [26], which lack the capability of bio-sensing. Although some integrated multi-parameter sensors have been investigated for the simultaneous detection of RI and flow rate, the compactness and stability of the entire system is decreased significantly [21].

In this paper, an integrated biological analysis and flow rate sensing based on Co^{2+} doped TFBG has been proposed and experimentally demonstrated for the detection of the B[a]P molecules. Due to the RI change of the immunoreactions between the B[a]P molecule and antibody on the surface of the TFBG, the B[a]P concentration can be measured by interrogating the wavelength interval between the cladding mode and core mode. Meanwhile, the Co^{2+}-doped fiber is self-heated by using a pump laser, and the flow rate is measured by using the wavelength shift of the core mode due to the heat exchange effect. The proposed fiber optic biosensor for the detection of B[a]P and flow rate have potential applications in studies of environment protection, medicine, and bioengineering, etc.

II. Preparation Principle of the Proposed Sensor

Due to the tilted angle in the TFBG with respect to the longitudinal axis of the fiber, the forward-propagating core mode can be coupled into the backward-propagating cladding modes. According to the phase matching conditions, the Bragg resonance wavelength λ_{Bragg} and the i^{th} cladding mode resonances wavelength $\lambda_{clad,i}$ are given by [27, 28]

$$\lambda_{Bragg} = 2n_{eff,core}\frac{\Lambda}{\cos\theta}. \tag{1}$$

$$\lambda_{clad,i} = (n_{eff,core} + n_{eff,clad,i})\frac{\Lambda}{\cos\theta}. \tag{2}$$

where $n_{eff,core}$ and $n_{eff,clad,i}$ are the effective refractive indices of the core mode and the cladding mode, respectively. Λ represents the grating period, while θ denotes the tilt angle between the crating plane and the vertical line of the fiber axis. Thus the wavelength interval between the core mode and cladding resonance wavelength can be expressed as

$$\lambda_{interval} = (n_{eff,core} - n_{eff,clad,i})\frac{\Lambda}{\cos\theta}. \tag{3}$$

For RI sensing, the well-known principle of the TFBG in the Co^{2+}-doped fiber is also similar to that in the SMF. The cladding modes are inherently very sensitive to the RI of the surrounding chemical sample due to the evanescent field of the cladding modes. However, the core mode of the TFBG is insensitive to the surrounding RI due to the confining of the optical field in the core of the Co^{2+}-doped fiber. Hence the wavelength interval change between the core mode and cladding mode resonance wavelength, $\Delta\lambda_{interval}(RI)$, can be expressed as

$$\Delta\lambda_{interval}(RI) = \Delta n_{eff,clad,i}(RI)\frac{\Lambda}{\cos\theta}. \tag{4}$$

where $\Delta n_{eff,clad,i}(RI)$ is the RI change of the cladding mode. Thus the TFBG can be implemented as an optical fiber biosensor platform. Immunoreactions between the antibody immobilized on the TFBG and the target B[a]P molecules could change the surrounding RI, which can be detected through the wavelength interval change.

For flow rate sensing, in the Co^{2+}-doped fiber, the pumped light can be absorbed and converted into heat due to the non-radiation effect; thus, the Co^{2+}-doped fiber can be heated through the pump light [24]. When the liquid sample flows through the fiber, the heat generated by the pumped light can be carried away from the Co^{2+}-doped fiber. According to the theory of hot-wire, the heat loss can be expressed as [23]

$$H_{power} = \Delta T_h(A + B\upsilon^k). \tag{5}$$

where H_{power} is the power absorbed by the heating element, ΔT_h is the temperature change of the Co^{2+}-doped fiber, υ is flow rate, A and B are empirical coefficients, and k is the exponent.

Due to the temperature change during the heat loss of the Co^{2+}- doped fiber, the wavelength shift of the core mode and the cladding mode is well known as [23]

$$\begin{aligned}\Delta\lambda_{Bragg} &= \lambda_{Bragg}\left(\frac{1}{n_{eff,core}}\frac{dn_{eff,core}}{dT} + \frac{1}{\Lambda}\frac{d\Lambda}{dT}\right)\Delta T \\ &= \lambda_{Bragg}(\alpha+\beta)\Delta T.\end{aligned} \tag{6}$$

$$\Delta\lambda_{clad,i} = \lambda_{clad,i}[\frac{1}{(n_{eff,core}+n_{eff,clad,i})}\frac{d(n_{eff,core}+n_{eff,clad,i})}{dT} + \frac{1}{\Lambda}\frac{d\Lambda}{dT}]\Delta T = \lambda_{clad,i}(\gamma+\beta)\Delta T. \quad (7)$$

where ΔT is the temperature change, $\alpha=(1/n_{eff,core})(dn_{eff,core}/dT)$ is the thermo-optic coefficient of the fiber core ($\sim 8.16\times10^{-6}K^{-1}$) [28], $\beta=(1/\Lambda)(d\Lambda/dT)$ is the thermal expansion coefficient of the fiber core ($\sim 5.5\times10^{-7}K^{-1}$) [29], and $\gamma=\frac{1}{(n_{eff,core}+n_{eff,clad,i})}\frac{d(n_{eff,core}+n_{eff,clad,i})}{dT}$ is the thermo-optic coefficient of the fiber cladding. The wavelength shift of core mode with the flow rate can be expressed as

$$\Delta\lambda_{Bragg} = \lambda_{Bragg}(\alpha+\beta)H_{power}/(A+B\upsilon^k). \quad (8)$$

Since the core mode is insensitive to the surrounding RI change, the flow rate can be measured through the Bragg wavelength without the interference of surrounding RI change.

However, besides the core mode, the cladding mode can be also modulated through the heated exchange induced by the flow rate. Hence the B[a]P detection interrogated by the wavelength interval may be affected by the flow rate. Therefore, the cross-sensitivity of the flow rate for the wavelength interval is also analyzed. The wavelength interval change with the temperature can be expressed as

$$\Delta\lambda_{interval} = \Delta\lambda_{Bragg} - \Delta\lambda_{clad,i} = [\lambda_{Bragg}\alpha + \lambda_{Bragg}\beta - \lambda_{clad,i}\gamma - \lambda_{clad,i}\beta]\Delta T. \quad (9)$$

Thus, one can deduce the expression of wavelength interval change and flow rate as

$$\Delta\lambda_{interval} = [\lambda_{Bragg}\alpha + \lambda_{Bragg}\beta - \lambda_{clad,i}\gamma - \lambda_{clad,i}\beta]H_{power}/(A+B\upsilon^k) \quad (10)$$

Since the thermo-optic coefficient difference between the fiber core (α) and cladding (γ) is less than 0.00324, the wavelength interval change can be rewritten as

$$\Delta\lambda_{interval} \approx (\lambda_{Bragg} - \lambda_{clad,i})(\alpha+\beta)H_{power}/(A+B\upsilon^k). \quad (11)$$

For the weakly TFBGs, the wavelength interval between the core mode and cladding mode is less than 30nm (shown in Fig. 1(a)). Given that H_{power}=1000 J, $A=0.15$, $B=0.0015$, k is 0.5 [30]. Hence the wavelength interval change with the flow rate range from 0 to 1 μL/s is given by

$$\Delta\lambda_{interval} < 30nm\times(8.16\times10^{-6}/K + 5.5\times10^{-7})(\frac{1000J}{0.15} - \frac{1000J}{0.15+0.0015}) = 0.017nm. \quad (12)$$

Eq. 12 shows that wavelength interval change between the core mode and cladding mode is very small with the flow rate range from 0 to 1 μL/s. Hence, the cross-sensitivity of the flow rate for the wavelength interval can be almost neglected. Therefore, the RI and the flow rate could be simultaneous measured through the Bragg wavelength and wavelength interval change, respectively, without the cross-talk. Thus in this experiment, the B[a]P is detected through wavelength interval change, while the flow rate is measured by interrogating the Bragg wavelength.

III. Fabrication of the TFBG inscribed in Co^{2+}-doped optical fiber

In the proposed sensor, a Co^{2+}-doped optical fiber was employed as the sensing fiber. The Co^{2+}-doped fiber has a core diameter of 8.4μm, which is efficient in converting light energy into heat at the wavelength of 1480 nm with an absorption coefficient of ~11.3 dB/cm. A section of the Co^{2+}-doped optical fiber with a length of 20 mm was spliced with two single mode fibers (SMFs). The fabrication of the TFBG in Co^{2+}-doped optical fiber is similar to that written in the SMF. The TFBG was inscribe into the Co^{2+}-doped optical fiber by using a KrF excimer laser (Coherent BraggStar) with a wavelength of 248 nm. Between the Co^{2+}-doped optical fiber and the laser, a phase mask was fixed on a rotation stage in order to adjust inclination angle in the perpendicular plane to the incident laser beam. The fibers were hydrogen-loaded for 10 days under a high pressure of ~11.0 MPa. According to the Ref. 27, a TFBG with an optimized tilt angle of 8° was written in the fiber with a length of 15mm. After the writing process, the TFBG was subjected to annealing at 80 °C for 24 h to remove the residual hydrogen.

The transmission spectrum of the Co^{2+}-doped TFBG was investigated first, as shown in Fig. 1. Obviously, it has a core mode resonance, several cladding mode resonances, and between them, the ghost mode resonance. The Co^{2+}-doped fiber should be short, and the TFBG must be closed to the two splicing points between Co^{2+}-doped fiber and SMF, because the power of light transmitted through the TFBG is also attenuated due to the high absorption of Co^{2+}-doped fiber.

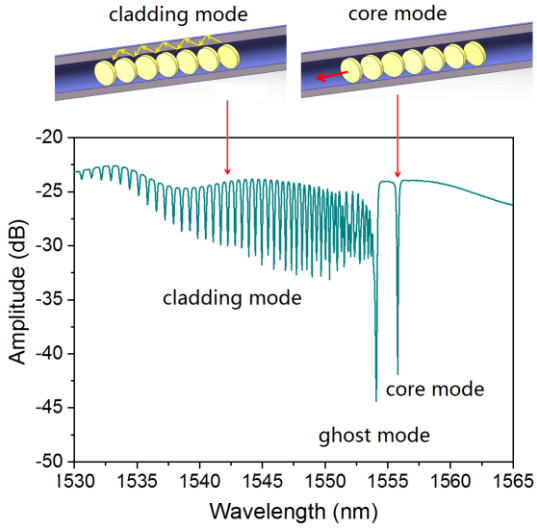

Fig. 1 The transmission spectrum of the TFBG.

The temperature response of the TFBG was measured by fixing the TFBG into a chamber, in which the temperature can be adjusted from 20°C to 260°C with a step of 30°C. Fig. 2(a) shows the transmission spectra at different temperature. The transmission dips of both the core mode and cladding mode shift to a longer wavelength as the temperature increases. Fig. 2(b) shows the relationship between the temperature and the core mode. The temperature sensitivity of the TFBG was measured as 7.6 pm/℃, which is similar to the response of TFBG on normal SMF. Then the Co^{2+}-doped TFBG was

This article has been accepted for publication in a future issue of this journal, but has not been fully edited. Content may change prior to final publication. Citation information: DOI 10.1109/JSEN.2019.2948964, IEEE Sensors Journal

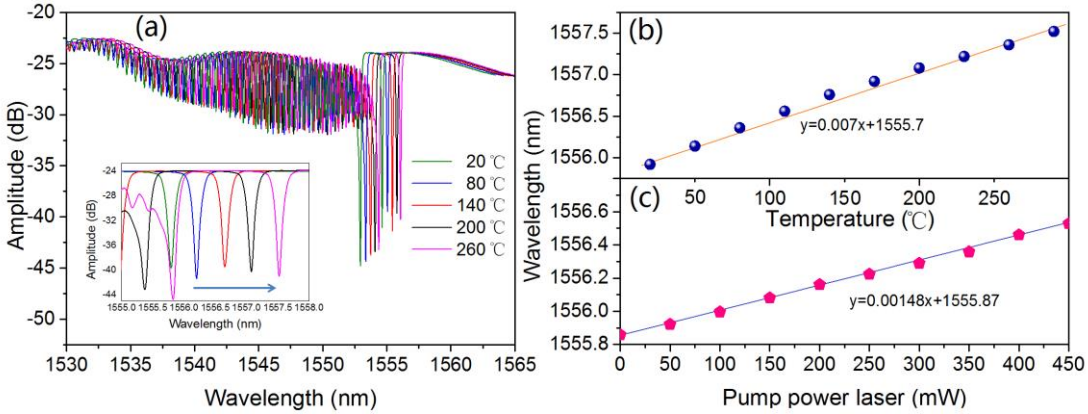

Fig. 2 (a) Transmission spectral of the TFBG with different temperature (b) The relationship between the wavelength of the core mode and temperature. (c) The relationship between the wavelength of the core mode and pump power laser.

injected with 1480-nm laser. The power of the laser is increased from 0 to 450 mW. Fig. 2(c) shows the relationship between the pump laser power and the core mode. The wavelength of the core mode exhibits the red shift with the increased laser power due to the absorption of laser power on Co^{2+}-doped fiber. The convention sensitivity is 1.48 pm/mW. Hence the maximum temperature can reach 95 ℃with the laser power of 450 mW according to the temperature sensitivity of 1.3℃/mW.

The RI response of the TFBG inscribed in Co^{2+}-doped optical fiber was experimentally measured at the room temperature (25℃). The microfluidic channel was injected with glycerin aqueous solutions with different concentrations, of which RI was ranged from 1.4057 to 1.4486 RIU (Abbe refractometer). In each measurement, the transmission spectrum was recorded until the glycerin aqueous solution was flown surround the entire TFBG, as shown in Fig. 3(a). The wavelength of the "cut-off mode," which is defined as the boundary between cladding and leaky modes (blue stars marked in Fig. 3(a)), is chosen to measure the RI of the liquid around the TFBG. The cut-off mode is identified by the first resonance (going toward short wavelengths) for which the out-of-resonance transmission (i.e., the transmission maxima on each side of the transmission dip) decreases below the baseline determined by the top level of the remainder of the spectrum on the long wavelength side, as shown in the inset of Fig. 3 (a) [31]. It is shown that as the surrounding RI changes, the cut-off mode is experienced a red-shift and a smoothing of the spectrum is observed, indicating that the coupling of the cladding modes was accelerated. On the contrary, only the core mode and the ghost mode remain. The wavelengths of the core modes are kept constantly within the RI range. In Fig. 3(b), a linear approximation between the cut-off mode and the wavelength interval between two cut-off cladding and core modes and RI can be adjusted in the RI range from 1.4057 to 1.4486 RIU, indicating that the RI sensitivity of -306.8 nm/RIU for the wavelength interval can be achieved.

IV. Experiments and Discussion

A. Experimental setup

The experimental setup is shown in Fig. 4(a). An amplified spontaneous emission with the wavelength of 1525-1565 nm and the output power of 20 mW was used to illuminate the Co^{2+}-doped TFBG. A 1480 nm tunable pump laser was also launched into the Co^{2+}-doped TFBG via a 1480/1550 wavelength-division multiplexer (WDM). The transmission spectrum of the Co^{2+}-doped TFBG was interrogated through an optical spectrum analyzer (OSA) (AQ6317B, YOKOGAWA Co., Ltd.) with the resolution of 0.02 nm. A linear polarizer and polarization controller (PC) were placed upstream of the TFBG to adjust the state of polarization of light. During the experiments, the chemical sample was injected into the inlet, passed through the sensing chamber, flown in the waste reservoir, and pulled out from the outlet. The flow rate of the chemical sample was adjusted precisely by using a syringe pump with polytetrafluoroethylene (PTFE) tubes, as shown in Fig. 4 (b). A pressure controller (OB1 MK3, Elveflow) contained with a pressure syringe pump was used in order to control the flow rate precisely. The flow rate can be measured by using an in-line PZT flow sensor (MFS3, Elveflow). The pressure controller could receive the feed-back signal from the PZT flow sensor and adjusted the output flow rate through a PID algorithm. Both the pressure controller and the PZT flow sensor form a closed-loop system, which keep the flow rate constant precisely.

The Co^{2+}-doped TFBG was slightly pre-stretched and placed in a PDMS-based microfluidic channel, as shown in Fig. 4(c). During the experiments, the sensors were fixed in PDMS-based micro-fluidic channels designed specifically for the biosensing tests. The width and height of the micro-channel are 220 μm and 180 μm, respectively. Hence the fiber could be placed into the micro-channel. The fiber axis was parallel to the solution flow. The two sides of the fiber in the inlet and outlet were fixed by using the UV-sensitive adhesive, as shown in Fig. 4 (b). Bio-sample solutions were injected into the micro-fluidic chip via an electronic- controlled pump.

First, the organic matter on the surface of the Co^{2+}-doped TFBG was clean off by using the piranha solution (H_2O_2:H_2SO_4=in a 1:3 ratio by volume). The microfluidic channel was washed with ultrapure water until the pH of the cleaning water reached neutral. After that, the microfluidic channel was filled with a 5% 8-aminopyrene-1,3, 6-trisulfonic acid, trisodium salt (APTS) solution with 5% HCL at 75° for 1 h in order to modify the surface of the Co^{2+}-doped TFBG with

This article has been accepted for publication in a future issue of this journal, but has not been fully edited. Content may change prior to final publication. Citation information: DOI 10.1109/JSEN.2019.2948964, IEEE Sensors Journal

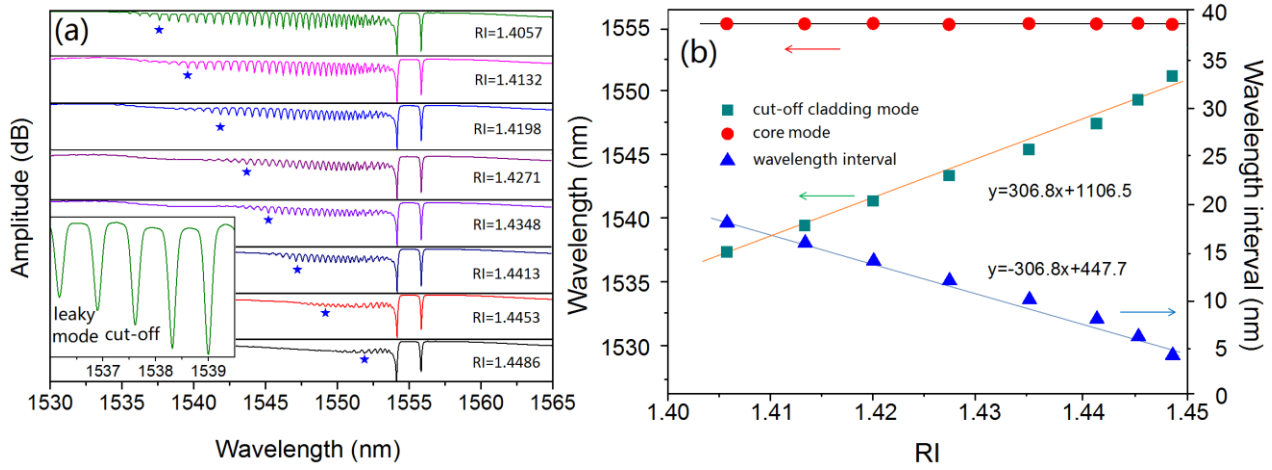

Fig. 3 (a) Transmission spectral of the TFBG with different surrounding RI. Inset shows the closed view of the spectrum with the RI of 1.4057. (b) Wavelength shift of core mode and cladding mode and the wavelength interval.

amine groups. After that, the glutaricdialdehyde solution with a concentration of 2.5% dissolved in the PBS buffer was injected into the microfluidic channel for 45 min, and cleaned twice using PBS and three times with ultrapure water. The Co^{2+}-doped TFBG was immersed with a 0.5mg/ml B[a]P mouse monoclonal antibody for 30 h, and the unbounded antibody was removed with the washing process of ultrapure water. In order to block protein to prevent non-specific binding on the surface of the Co^{2+}-doped TFBG, a 2mg/ml BSA solution was also deposited. Finally, a goat anti-mouse IgG conjugated with fluorescein isothiocyanate (FITC) was also pumped into the Co^{2+}-doped TFBG to associate with the B[a]P antibody, followed by the washing process. Fig. 4 (d) shows the fluorescent image of the Co^{2+}-doped TFBG with anti-mouse IgG-FITC. Obviously, the fluorescence microscopy confirms that the B[a]P antibody was immobilized on the surface of the Co^{2+}-doped TFBG uniformly.

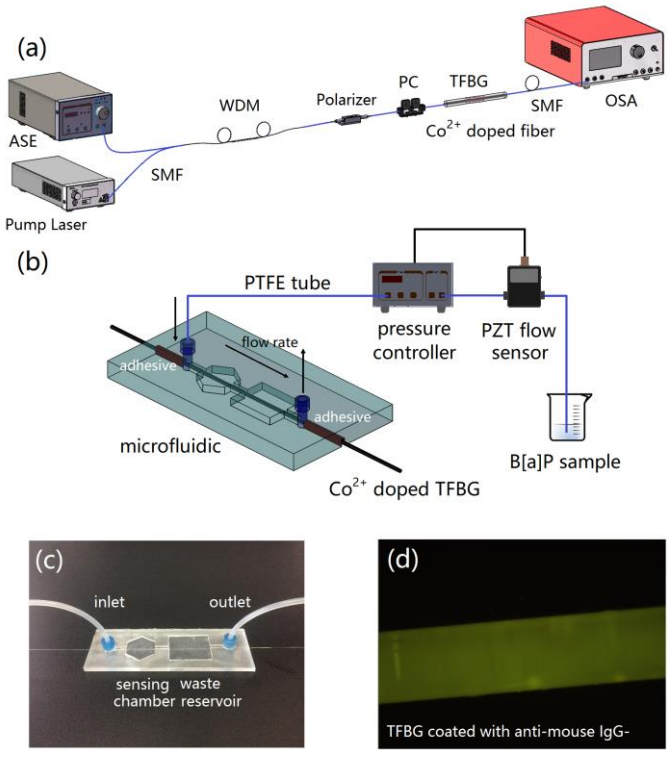

Fig. 4. (a) The experimental setup of the proposed sensor. (b) The detail experimental setup of the flow rate controller. (c) PDMS-based microfluidic channel. (d) The fluorescent image of the Co2+-doped TFBG with anti-mouse IgG-FITC.

B. The measurement of the B[a]P with different concentrations

Fig. 5 (a) and (b) show the transmission spectra of cut-off cladding mode and core mode for the modification and associated events before and after rinsing. The wavelength shifts of the core mode and cut-off mode and the wavelength interval between two modes are shown in Fig. 5(c). The initial wavelength of the cut-off cladding mode at 1537.34 nm undergoes a red shift as a consequence of the adsorption of additional layers on the surface of the Co^{2+}-doped TFBG due to the large RI change at each surface event before and after rinsing. Then a B[a]P solution with the concentration of 110 pM was injected into the microfluidic channel with 2 min followed with the repeated washing process to remove the unassociated B[a]P molecular. The immunoreaction between the antibody and the B[a]P was occurred after the injection, and the cut-off cladding mode shifts from 1537.48 nm to 1537.54 nm. However, the core mode was fixed at the wavelength of 1555.82nm. Hence the wavelength interval is decreased from 18.49nm to 18.43nm. Thus the B[a]P solution can be detected through the wavelength interval between the core mode and cut-off cladding mode.

B[a]P solutions with concentrations of 90 pM, 100 pM, 110 pM, 150 pM, 200 pM, 500 pM, and 1000 pM were injected into the microfluidic channel with the flow rate of 0.2 μL/s. The Co^{2+}-doped TFBG was kept for 35s in order to associate the B[a]P molecule with the antibody completely, then followed by the washing process of 15s. Fig. 5(d) shows the wavelength interval change of the TFBG with different concentrations of B[a]P solution, which indicates the specific associations between the B[a]P molecule and antibody. After each measurement, the TFBG was injected into pepsin solution to remove the associated B[a]P molecules. With the washing process of 10s, the wavelength interval change was returned back to the baseline because the associated B[a]P molecules was released. In addition, from Fig. 5(d) it can be seen that the wavelength interval is not changed when the B[a]P solution

This article has been accepted for publication in a future issue of this journal, but has not been fully edited. Content may change prior to final publication. Citation information: DOI 10.1109/JSEN.2019.2948964, IEEE Sensors Journal

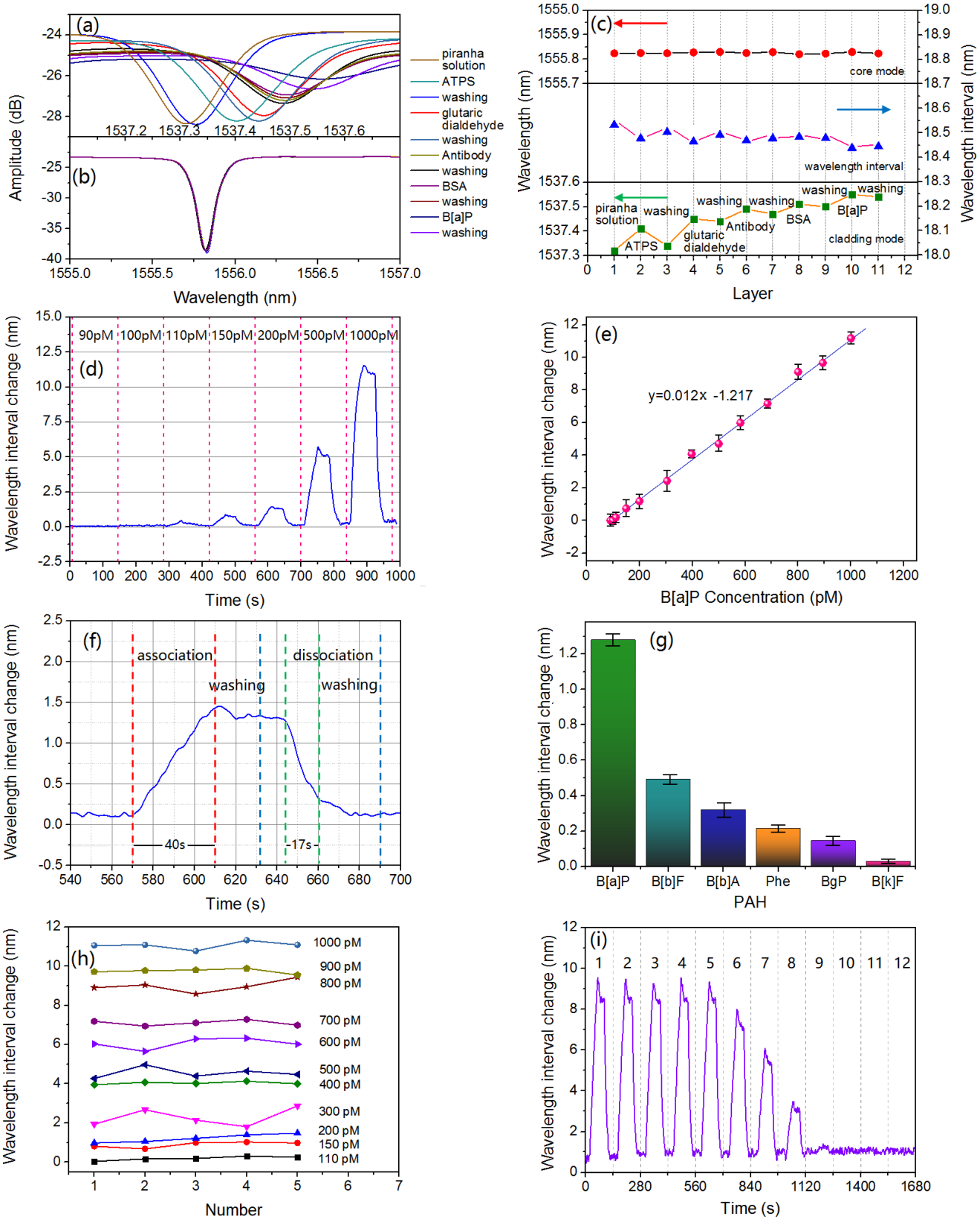

Fig. 5. The transmission spectra with the glutaricdialdehyde, antibody, BSA, and B[a]P. (a) cut-off cladding mode (b) core mode. (c) Wavelength shift of cut-off cladding mode and core mode, and the wavelength interval. (d) The wavelength shift of the TFBG with different concentrations of B[a]P solution. (e) The relationship between the wavelength shift and the concentration of B[a]P solution. (f) The time response of the TFBG. (g) Wavelength shift for the other PAH sample. (g) The selectivity of the Co2+-doped TFBG. (h) The repeatability of the Co2+-doped fiber sensor. (i) the reusability of the Co2+-doped fiber sensor.

concentrations lower than 110 pM. Therefore, the limit of detection of the Co^{2+}-doped TFBG is achieved as 110pM. Meanwhile, the linear fitting curve for the wavelength interval change is $y = 0.012x - 1.217.$, hence the sensitivity of 12pm/pM for the Co^{2+}-doped TFBG is achieved, as shown in Fig. 5(e).

The time response of the sensor has been analyzed. An enlarged view of the wavelength interval change is shown in Fig. 5(f). From 540 to 600s, the B[a]P solution with the concentration of 200pM was pumped into the Co^{2+}-doped TFBG. The wavelength interval began to change 1.28 nm, hence the association procedure of early 40 s was achieved. The wavelength interval change remained at 1.28 nm for about 10s after a washing process, and began to decrease for 17 s when the Co^{2+}-doped TFBG was washed with pepsin solution and ultrapure water.

The selectivity of the Co^{2+}-doped TFBG was also researched with 5 different PAHs with the same concentration of 200 pM, which may interfere the response of the Co^{2+}-doped TFBG due to the similar molecular weight. 5 different PAHs solution were injected into the Co^{2+}-doped TFBG in sequence and washed for 10 s until the wavelength interval returned back to the baseline. The cross-reactivity is defined as the ratio between the wavelength interval measured with PAHs solution and B[a]P solution ($C = \lambda_{PAH} / \lambda_{B[a]P} \times 100\%.$), as shown in Fig. 5(g). Although Benzo[b]fluoranthene (48.3%) induce a dramatic wavelength interval change of the sensor due to the similar number of condensed aromatic rings, the wavelength interval change of other four PAHs are very small.

The repeatability of the proposed Co^{2+}-doped fiber sensor was also researched. B[a]P solutions with concentrations from 110 pM to 1000 pM were tested in sequence, as shown in Fig. 5(h). In each single concentration, the B[a]P solution was measured with 5 times. After each measurement, the microfluidic channel was injected into pepsin solution to remove the B[a]P. The maximum standard variation is 23.2% with the concentration of 300pM, and the minimum standard variation is 2.1% with the concentration of 400pM.

In order to research the reusability of the sensor, B[a]P solutions with concentrations of 800 pM were injected into the microfluidic channel repeatedly. In each measurement, the solution was kept for 20 s in order to allow all the B[a]P molecules in the solution to bind completely to the immobilized antibodies, then followed by a 20 s washing in ultrapure water. After each measurement, the microfluidic channel was injected into pepsin solution to remove the B[a]P, followed by washing in ultrapure water. Fig. 5(i) shows the response of the sensor with the concentration of 800 pM. It can be seen that in the initial 5 measurements, the wavelength interval change remained at almost 8.24 nm. However, for the subsequent 3 measurements, the wavelength interval change began to decrease sequentially. After the 9th measurement, the wavelength interval change was almost fixed without any change, indicating the degradation of the antibody induced by the pepsin. Hence the reusability of the proposed Co^{2+}-doped TFBG is 8 times.

C. The flow rate response of the sensor

The Co^{2+}-doped fiber can be heated through the pumped light with the non-radiation effect. Fig. 6(a)-(e) show the thermography of the Co^{2+}-doped fiber heated by using the pumped light power of 450, 400, 300, 200, and 100 mW with the wavelength of 1480nm. It can be seen that the temperature of the Co^{2+}-doped fiber is changed at different pumped light power. Fig. 6(f) shows the relationship between the temperature of the Co^{2+}-doped fiber and the pumped light power. The wavelength shift of the core mode is increased with the increasing of the pumped light power. The sensitivity of the wavelength shift is achieved as 0.0015 nm/mW, proving the nonradiative absorption of the Co^{2+}-doped fiber.

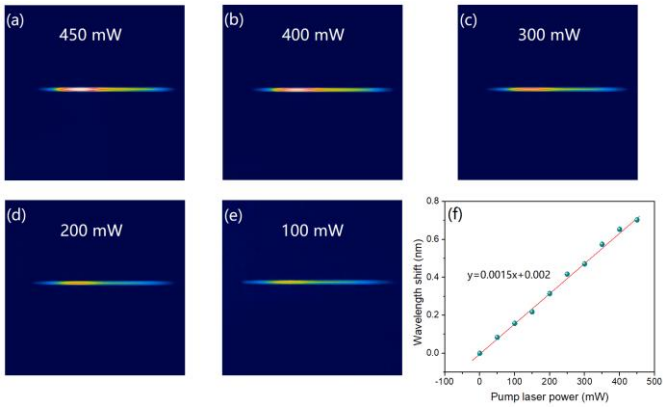

Fig. 6.The thermographic camera of the Co^{2+}-doped fiber heated by using the pumped light power of (a) 450mW, (b) 400mW, (c) 300mW, (d) 200mW, and (e) 100 mW. (f) The relationship between the wavelength shift of the core mode.

The flow rate measurement of the Co^{2+}-doped TFBG was investigated with the range from 0 to 1.03μL/s. The heating laser intensity was set as 450 mW. Due to the increasing of the temperature, the wavelength for both the core mode and cladding mode experience a red-shift. The flow rate of a B[a]P solution with the concentration of 110 pM was adjusted from 0 to 1.03 μL/s by using a syringe pump. Noted that the flow rate was calibrated by calculating the mean value in each measurement through the PZT flow sensor. For example, in the measurement of 1.03 μL/s in Fig. 7 (d), the calibrated flow rate (1.03 μL/s) is the mean value of the measured flow rate through the PZT flow sensor from 480s to 510s. The transmission spectra of the cut-off cladding mode and core mode are shown in Fig. 7 (a) and (b).The wavelength shift with the flow rate change for the cut-off cladding mode and core mode and the wavelength interval between two modes are shown in Fig. 7(c). Although the cut-off cladding mode and core mode shifted to the shorter wavelengths simultaneously, it can be observed that the wavelength interval is almost fixed, as shown in Fig. 7(c). The standard variation of the wavelength difference is only 0.02 nm in the flow rate range from 0 to 1.03 μL/s. Therefore, the wavelength interval could discriminate the flow rate and the surrounding B[a]P molecule. It is shown that the wavelength shift of the core mode keeps a good quadratic relationship with the flow rate. The maximum sensitivity of -0.13 nm/(μL/s) was achieved with the flow rate of 1.03μL/S, as shown in Fig. 7(c). Besides, the wavelength change with the flow rate from 0 μL/s to 1.03 μL/s is shown in Fig. 7(d). The response time of 15.42

This article has been accepted for publication in a future issue of this journal, but has not been fully edited. Content may change prior to final publication. Citation information: DOI 10.1109/JSEN.2019.2948964, IEEE Sensors Journal

s

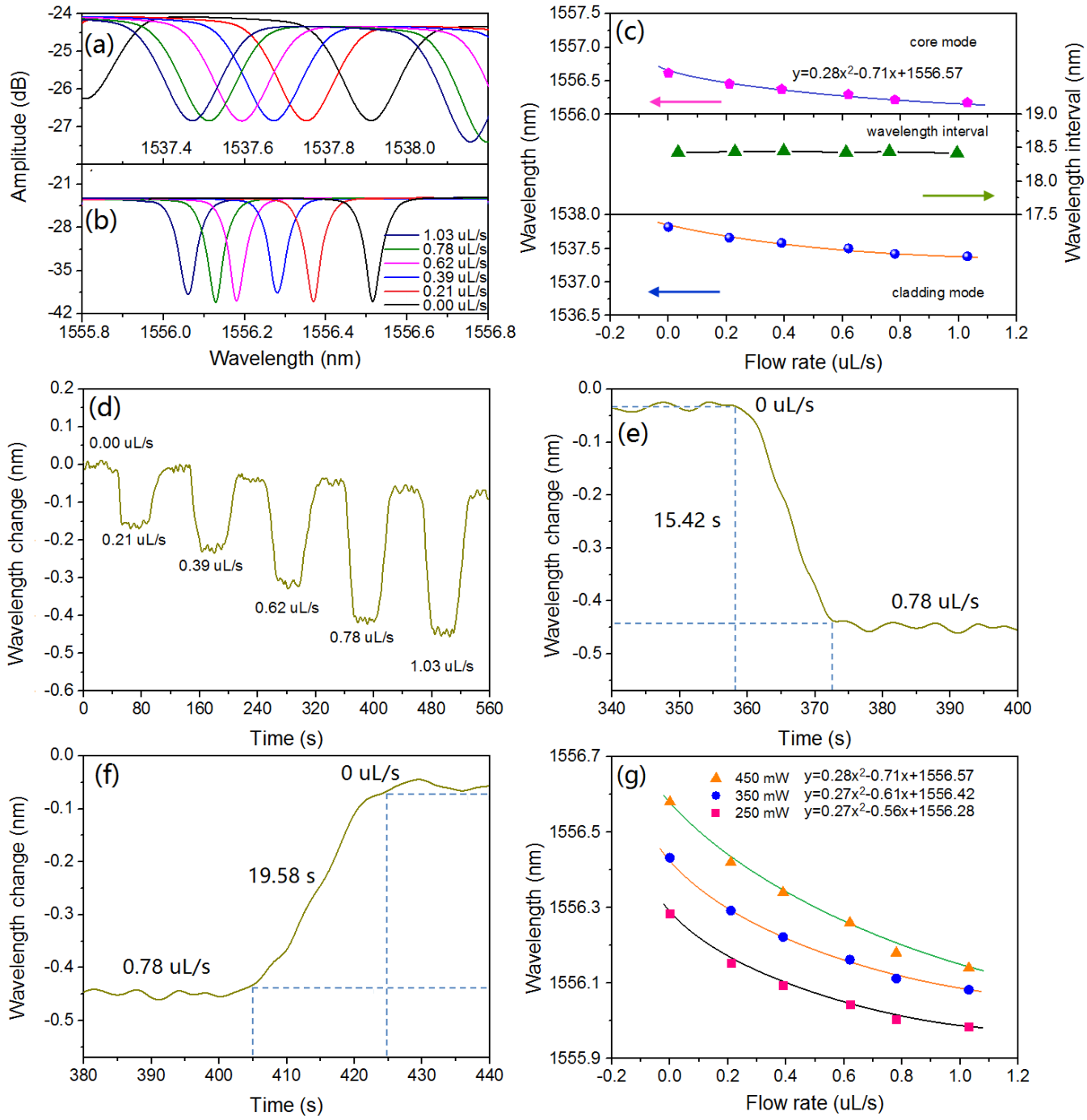

Fig. 7. The transmission spectra with different flow rate. (a) cut-off cladding mode (b) core mode. (c) Wavelength shift of cut-off cladding mode and core mode, and the wavelength interval. (d) The wavelength change of the TFBG with different flow rates. (e) The time response of the TFBG. (f) the recovery time of the TFBG. (g) Wavelength shift of core mode with different powers of pump laser.

was measured with the flow rate from 0 μL/s to 0.78 μL/s, as shown in Fig. 7 (e). At the same time, the wavelength change with the flow rate from 0.78 μL/s back to 0μL/s is shown in Fig. 7(f). The recovery time of 19.58 s was measured. Fig. 7 (g) shows the wavelength shift of the core mode at different heating laser intensity. It is can be seen that the sensitivity was increased significantly with the increasing of the heating intensity.

The ambient temperature is a key cross-sensitivity for the proposed sensor. With regard to the B[a]P measurement, the temperature change could influent the immunoreaction between the antibody and the B[a]P molecular. The high temperature may even make the denaturation of the antibody and decomposition of the B[a]P molecules, resulting in the inaccuracy of the measurement. With regard to the flow rate detection, the temperature change could also make a wavelength shift of the core mode due to the change of the refractive index and period of the TFBG. Hence the ambient temperature should be controlled in order to improve the accuracy of the sensor. During the experiments, the entire microfluidic and the Co^{2+}-doped TFBG were fixed into an

environmental chamber (TH-G, JeioTech), which could control the ambient temperature with the variation of 0.3 ℃.

V. Conclusion

In conclusion, we have demonstrated an integrated biological analysis and flow rate sensing based on Co^{2+} doped tilted fiber Bragg gratings for the detection of the Benzo[a]pyrene molecules. A TFBG with a tilted angle of 8° was inscribed into a Co^{2+}-doped. Due to the self-heated by a pump laser, the core mode of the Co^{2+}-doped TFBG was interrogated to measure the flow rate according to the heat exchange, acting as a "hot-wire" sensor. Meanwhile, based on the evanescent field of the cladding mode, the immunoreaction between the target B[a]P and the antibody can be detected by interrogating the wavelength interval between core mode and cut-off cladding mode. Experimental results show that the real-time measurement sensitivities of 12 pm/pM and -0.13 nm/(μL/s) for the Benzo[a]pyrene detection and flow rate were achieved, respectively. The proposed flow rate compensated fiber optic B[a]P biosensor have potential applications in studies of environment protection, medicine, and bioengineering, etc.

References

[1] M. D. Carlo, M. D. Marcello, M. Giuliani, M. Sergi, A. Pepe, D. Compagnone, "Sensitive immunosensor for benzo[a]pyrene detection based on dual amplification strategy of PAMAM dendrimer and amino-modified methylene blue/SiO_2 core-shell nanoparticles," *Biosens. Bioelectron.* vol. 26, no. 9, pp. 3761-3767, Nov. 2011.

[2] H. Shemer, K. G. Linden, "Aqueous photodegradation and toxicity of the polycyclic aromatic hydrocarbons fluorene, dibenzofuran, and dibenzothiophene," *Water Res.* vol. 41, no. 4, pp. 853 – 886, Dec. 2007.

[3] U.S. Environmental Protection Agency. Polynuclear Aromatic Hydrocarbons, U.S. EPA Method 610; Environmental Monitoring and Support Laboratory: Cincinnati, OH, July 1982.

[4] The Council of the European Union, The European Drinking Water Directive (98/83/EC): UK., Nov. 1998.

[5] National Health and Family Planning Commission of the P. R. C., Standardization Administration of the P. R. C.. Standards for Drinking Water Quality: Beijing, July 2006.

[6] L. Bao, P. Sheng, J. Li, S. Wu, Q. Cai, S. Yao, "Surface enhanced Raman spectroscopic detection of polycyclic aromatic hydrocarbons (PAHs) using a gold nanoparticles-modified alginate gel network," *Analyst* vol. 137, no. 17, pp. 4010-4015, Jul. 2012.

[7] M. Liu, Q. X. Li, G. A. Rechnitz, "Flow injection immunosensing of polycyclic aromatic hydrocarbons with a quartz crystal microbalance," *Anal. Chim. Acta* vol. 387, no. 1, pp. 29-38, Apr. 1999.

[8] K. V. Gobi, M. Sasaki, Y. Shoyama, N. Miura, "Highly sensitive detection of polycyclic romatic hydrocarbons (PAHs) and association constants of the interaction between PAHs and antibodies using surface plasmon resonance immunosensor" *Sens. Actuators B Chem.* vol. 89, no. 2, pp. 137-143, Mar. 2003.

[9] N. Miura, M. Sasaki, V. Gobi, C. Kataoka, Y. Shoyama, "Highly sensitive and selective surface plasmon resonance sensor for detection of sub-ppb levels of benzo[a]pyrene by indirect competitive immunoreaction method," *Biosens. Bioelectron* vol. 18, no. 7, pp. 953-959, Jul. 2003.

[10] J. F. Fernández-Sánchez, A. C. Segura, C. Blanco, A. F. Gutiérrez, "Highly sensitive and elective fluorescence optosensor to detect and quantify benzo[a]pyrene in water samples," *Anal. Chim. Acta* vol. 506, no. 1, pp. 1-7, Oct. 2004.

[11] L. Wang, X. M. Wan, R. Gao, D. F. Lu, Z. M. Qi, "Nanoporous Gold Films Prepared by a Combination of Sputtering and Dealloying for Trace Detection of Benzo[a]pyrene Based on Surface Plasmon Resonance Spectroscopy," *Sensors* vol. 17, no. 6, pp. 1255, Jun. 2017.

[12] B. Luo, Z. Yan, Z. Sun, J. Li, and L. Zhang, "Novel glucose sensor based on enzyme-immobilized 81° tiltedfiber grating," *Opt. Express* vol. 22, no. 25, pp. 30571 – 30578, Dec. 2014.

[13] A. Ricciardi, A. Crescitelli, P. Vaiano, G. Quero, M. Consales, M. Pisco, E. Esposito, and A. Cusano, "Lab-on-fiber technology: a new vision for chemical and biological sensing," *Analyst* vol. 140, pp. 8068–8079, Jun. 2015.

[14] P. Vaiano, B. Carotenuto, M. Pisco, A. Ricciardi, G. Quero, M.Consales, A. Cusano, "Lab on Fiber Technology for biological sensing applications," *Laser & Photonics Reviews* vol. 10, no. 6, pp. 922–961, Dec. 2014.

[15] J. Li, Y. X. Zhou, Y. X. Guo, G. Y. Wang, R. R. J. Maier, D. P. Hand, W. N. MacPherson, "Label-free ferrule-top optical fiber micro-cantilever biosensor," *Sens. Actuators A: Phys.* vol. 280, pp. 505-512, Jul. 2018.

[16] N. J. Alberto, C. A. Marques, J. L. Pinto, and R. N. Nogueira, "Three-parameter optical fiber sensor based on a tilted fiber Bragg grating," *Appl. Opt.* vol. 49, no. 31, pp. 6085-6091, Jun. 2010.

[17] B. B. Luo, S. X. Wu, Z. G. Zhang, W. G. Zou, S. H. Shi, M. F. Zhao, N. B. Zhong, Y. Liu, X. Zou, L. L. Wang, W. N. Chai, C. M. Hu, and L. Zhang, "Human heart failure biomarker immunosensor based on excessively tilted fiber gratings," *Biomedical Opt. Express* vol. 8, no. 1, pp. 57-67, Dec. 2017.

[18] C. Ribaut, M. Loyez, J. C. Larrieu, S. Chevineau, P. Lambert, M. Remmelink, R. Wattiez, C. Caucheteur, "Cancer biomarker sensing using packaged plasmonic optical fiber gratings: Towards in vivo diagnosis," *Biosens. Bioelectron* vol. 15, no. 92, pp. 449-456, Jun. 2016.

[19] A. L. Aldabaa, Á. G. Vila, M. Debliquy, M. L. Amo, C. Caucheteur, D. Lahem, "Polyaniline-coated tilted fiber Bragg gratings for pH sensing," *Sens. Actuators B Chem.* vol. 254, no. 1, pp. 1087-1093, Jun. 2018.

[20] S. K. Duggal, K. Bucholz, "Effects of immobilization on intrinsic kinetics and selectivity of trypsin," *European journal of applied microbiology and biotechnology* vol. 16, no. 2, pp. 81-87, Jun. 1982.

[21] J. Sadeghi, A. B. Ghasemi, H. Latifi, "A Label-Free, Infrared Opto-Fluidic Method for Real-Time Determination of Flow Rate and Concentration with Temperature Cross-Sensitivity Compensation," *Lab Chip* vol. 16, no. 20, pp. 3957–3968, Aug. 2016.

[22] S. L. Stott, C. H. Hsu, D. I. Tsukrov, M. Yu, D. T. Miyamoto, B. A. Waltman, S. M. Rothenberg, A. M. Shah, M. E. Smas, G. K. Korir, F. P. Floy, A. J. Gilman, J. B. Lord, D. Winokur, S. Springer, D. Irimi, S. Nagrath, L. V. Sequist, R. J. Leed, K. J. Isselbacher, S. Maheswaran, D. A. Haber, and M. Toner, "Isolation of circulating tumor cells using a microvortex-generating herringbone-chip," *Proc Natl Acad Sci USA* vol. 107, no. 43, pp. 18392–18397, Oct. 2010.

[23] T. Chen, Q. Wang, B. Zhang, R. Chen, and K. P. Chen, "Distributed flow sensing using optical hot -wire grid," *Opt. Express* vol. 20, no. 8, pp. 8240-8249, Mar. 2012.

[24] S. Gao, A. P. Zhang, H. Y. Tam, L. H. Cho, and C. Lu, "All-optical fiber anemometer based on laser heated fiber Bragg gratings," *Opt. Express* vol. 19, no. 11, pp. 10124-10130, May. 2011.

[25] X. H. Wang, X. Y. Dong, Y. Zhou, K. Ni, J. Cheng, and Z. M. Chen, "Hot-wire anemometer based on silver coated fiber Bragg grating assisted by no-core fiber," *IEEE Photon. Technol. Lett.* vol. 25, no. 24, pp. 2458 – 2461, Dec. 2013.

[26] G. Liu, M. Han, and W. Hou, "High-resolution and fast-response fiber-optic temperature sensor using silicon Fabry-Pérot cavity," *Opt. Express* vol. 23, no. 6, pp., 7237-7247, Mar. 2015.

[27] T. Wang, K. Liu, J. F. Jiang, M. Xue, P. X. Chang, and T. G. Liu, "Temperature-insensitive refractive index sensor based on tilted moiré FBG with high resolution," *Opt. Express* vol. 25, no. 13, pp. 14900-14909, Jun. 2017.

[28] W. Wang, Y. Yu, Y. Geng, and X. Li, "Measurements of thermo-optic coefficient of standard single mode fiber in large temperature range," in International Conference on Optical Instruments and Technology (International Society for Optics and Photonics, 2015), paper 96200Y.

[29] S. Takahashi and S. Shibata, "Thermal variation of attenuation for optical fibers," J. Non-Cryst. Solids vol. 30, no. 3, pp. 359 – 370, Jan. 1979.

[30] Z. Y. Liu, M. L. V. Tse, A. P. Zhang, and H. Y. Tam, "Integrated microfluidic flowmeter based on a micro-FBG inscribed in Co^{2+}-doped optical fiber," *Opt. Lett.* vol. 39, no. 20, pp., 5877 – 5881. Nov. 2014.

[31] W. J. Zhou, D. J. Mandia, S. T. Barry, and J. Albert, "Absolute near-infrared refractometry with a calibrated tilted fiber Bragg grating," *Opt. Lett.* vol. 40, no. 8, pp., 1713-1716. Apr. 2015.

Ran Gao received his PhD degree in Electronic Science and technology from Beijing Institute of technology, China, in 2015. His research interests include fiber optical sensors, optical waveguide, and measurement instruments.

Jiansen Ye received his PhD degree in Electronic Science and technology from Beijing Institute of technology, China, in 2016. His research interests include fiber optical sensors, Embedded system, and measurement instruments.

Xiangjun Xin was born in Hebei, China, in 1969. He received the Ph.D. degree from the School of Electrical Engineering, Beijing University of Posts and Telecommunications (BUPT), Beijing, China, in 2004. He is currently a Professor with Advanced Research Institute of Multidisciplinary Science, Beijing Institute of Technology. His main research interests focus on broadband optical transmission technologies, optical sensor, and all-optical networks. Within this area, he has published over 60 SCI papers.